Sensor Placement Study for Online Flow Monitoring in Liquid Composite Molding

SYLVIA R. M. KUEH *and* SURESH G. ADVANI

Department of Mechanical Engineering
University of Delaware
Newark, DE 19716-3140

RICHARD S. PARNAS*

Polymers Division
100 Bureau Dr., Stop 8543
National Institute of Standards and Technology
Gaithersburg, MD 20899-8543

On-line sensing can play an important part in controlling the quality of the final product in any manufacturing environment, including liquid composite molding (LCM). Having a sensor embedded within the part itself is often the most effective means of monitoring its condition at various stages of manufacturing and even throughout its useful life. However, given their intrusive nature, there are practical limitations imposed upon their size, quantity and trajectory within the part. This study explores the possibility of using a single lineal sensor to monitor the resin flow front during the mold filling stage of LCM, and to detect the onset of void formation and the presence of dry spots within the mold. Experiments were conducted to characterize the response of a fiber optic system previously developed for cure monitoring. Simulations were then performed to determine the optimal placement of just one such sensor in a mold to demonstrate that sufficient information on the mold filling process could be obtained. The purpose of the simulation work was to learn how to interpret the sensor response and, subsequently, use it to control the LCM process.

INTRODUCTION

Liquid composite molding (LCM) has become a widely used polymer composite manufacturing process largely due to its versatility, fast cycle times and relatively low costs. However, there still remain many indeterminant parameters associated with the process such as local variations in permeability due to inhomogeneities in the preform and preform fit inside the mold cavity. Optimization of process conditions is typically empirically achieved by conducting molding experiments (1–6), which are not only time-consuming, but also expensive. Hence, there is a growing interest in the development of other means of both optimizing manufacturing parameters and enhancing understanding of how these parameters physically govern the outcome of the part at each stage of the process through simulations and in-situ monitoring (7–21).

To date, there exist a myriad of simulation packages and sensory devices explicitly designed for this purpose (7, 15–16, 22–26). An example of such a sensory system that has been successfully developed is Kranbuehl, *et al.*'s Frequency Dependent Electromagnetic Sensing system, which is capable of monitoring the progress of cure reactions, and the location and magnitude of maximum flow, through capacitance and frequency measurements (12). Another example is Fink *et al.*'s SMART weave system that also incorporates flow and cure monitoring capabilities based on voltage and resistance measurements (10). Third, there is also the real-time electronic sensing system developed by Kikuchi *et al.* (4).

The main appeal of on-line sensing is that it enables the appropriate corrective measures to be taken during

*Correspondence author.

manufacturing and thus, save the part from being rejected due to manufacturing defects. One of the most frequently encountered problems in LCM is the occurrence of voids or dry spots in the part. These are typically the result of air entrapment in the mold or imperfect impregnation of the preform (14). By monitoring the resin flow front during mold filling, it should be possible to detect the onset of a dry spot and, subsequently, take the necessary steps to correct the situation during the process.

While embedded on-line sensors are one of the best means of assessing what is happening within the mold, they often present additional complications as they themselves can become part of the inhomogeniety in the preform structure. However, these complications can be assuaged by having as few of these sensors present in the mold as possible, ideally only one, and also making them as small as possible. Therefore, it is not surprising many researchers have expressed optimism about using fiber optic sensors in composite manufacturing (11, 13, 20, 27–36). Previous experiments with fiber optic sensors embedded in glass preforms have been successfully used to detect resin arrival during the mold filling process (7).

In this work, a previously developed evanescent wave fluorescence (EWF) fiber optic cure monitoring system was adapted to provide an example of one type of technology that may provide the unobtrusive sensor required. The current form of the EWF sensor system detects fluorescent light from fluorophores dissolved in the resin. Standing (evanescent) waves at the fiber-resin interface excite fluorophores in the immediate vicinity, causing them to fluoresce (20, 27, 28). Some of the fluorescence then couples back into the optical fiber and propagates to the detection system. The evanescent field arises from the total internal reflection at the interface of the fiber and the surrounding medium, and extends beyond the reflecting interface into the surrounding medium, decaying exponentially in amplitude from that interface (37–44). In the past, researchers have found a linear correlation between the intensity of fluorescence measured from an EWF sensor and the length of fiber covered by the liquid containing the fluorescent dye for lengths less than 0.64 m (13, 34, 36, 45–46). To date, EWF sensors have been successfully used in cure monitoring of thermoset polymer composites (13, 20, 28–36), pH sensors (45) and in antigen-antibody binding studies (47, 48).

In this work, the fiber optic sensor response for fiber lengths exceeding 1 m was characterized through a series of idealized experiments. The results of these experiments were then employed to conduct a sensor simulation study for LCM in a square mold, with and without inserts. It is acknowledged that the bare fiber sensor system used for cure monitoring will not work for flow monitoring in a real molding environment due to effects such as microbending and intimate contact of the bare fiber with the surrounding reinforcing fibers. However, an improved optical fiber sensor with a response function that is as simple as the one illustrated below is expected to be suitable in molding environments, and is currently in development.

The main purpose of this paper is to demonstrate a concept: the feasibility of distinguishing mold filling anomalies based on information gathered from a single lineal sensor, such as an improved EWF system. This investigation aims to develop an understanding of how to interpret an EWF fiber optic sensor response, and, subsequently, how to use it to control the LCM process. Specifically, the goal is to understand these responses and address the issue of sensor placement so as to obtain as much information as possible about the flow pattern within the mold from a single sensor. Hence, the strategies for evaluating and interpreting each sensor response are applicable to any sensor which possesses either this linearly proportional response to changes in its environment or some other easily interpretable response function.

EXPERIMENTAL PROCEDURE AND RESULTS

The experimental apparatus used to conduct the fiber characterization experiments consists of a spectrometer and a 1.22 m long glass tube connected to a dye reservoir on one side and waste discharge on the other, as shown in *Fig. 1*. The spectrometer comprises an Ar^+ laser with integrated optics attached, a CCD camera and a computer. The optical arrangement attached to the laser contains two filters and a beam splitter. The detailed optical arrangement involved has been described previously (30).

A bare optical fiber was strung tautly through the corks at the two ends of the glass tube and held in place with 5-minute epoxy. The fiber was drawn from F2 Schott glass which has a refractive index of 1.62 and then coated with a polyvinyl acetate buffer for ease of handling and storage. The buffer was removed using spectral grade acetone before the commencement of each experiment. The bottom end of the bare fiber was then coupled with the spectrometer using a quick-connect fiber-holder.

The liquid level in the tube was driven by gravity and controlled using a three-way stopcock. Aqueous Rhodamine B solution, which fluoresces at wavelengths near 590 nm, was used in these experiments. As the dye solution fills the tube, scans were taken at every 0.05 m of liquid height, from 0 m to 1.17 m. Five scans were taken at each interval to account for any inherent fluctuations in light intensity. Ambient light is accounted for by subtracting, from each scan, the background reading, which was taken at the beginning of the filling experiment. Maximum intensities from the corrected scans were then plotted against the liquid column height or equivalently, the length of fiber covered by the liquid. These filling experiments were conducted for a dye concentration of 10^{-5}mol/L using a 100 μm-diameter fiber.

As can be seen in *Fig. 2*, the maximum fluorescence intensity from the sensor is approximately linearly

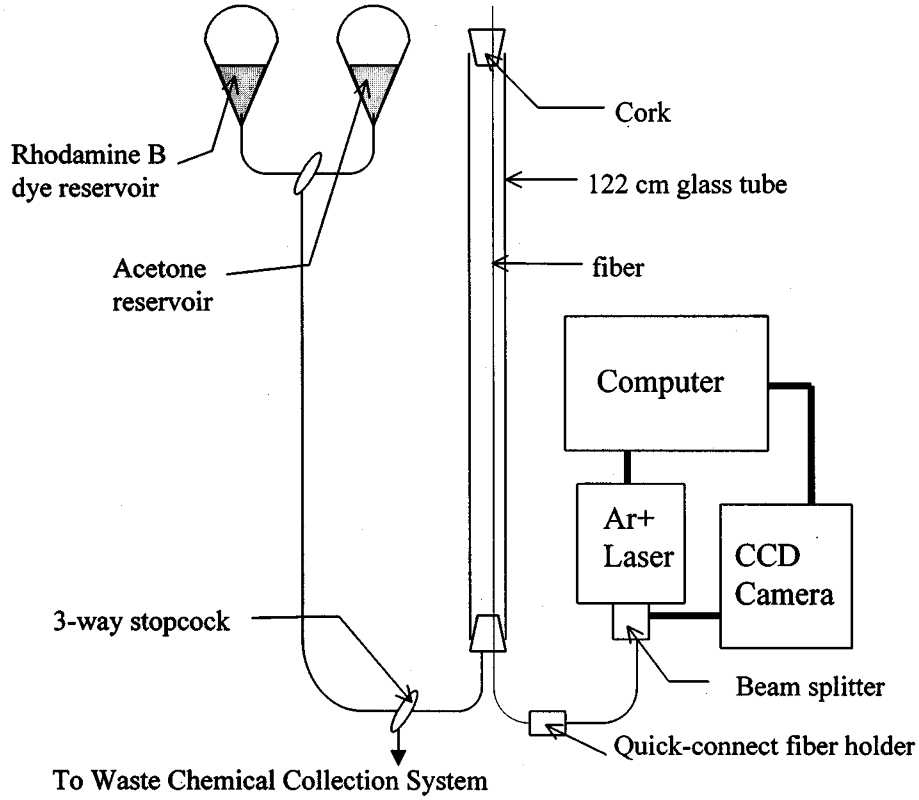

Fig. 1. Schematic of the experimental setup for fiber characterization experiments.

proportional to the length of fiber covered by the dye throughout its 1.17 m length. This is in agreement with the results from other studies in the literature which explored the relationship between the optical interaction between a fiber sensor and fluid surrounding it (13, 31–36) even though these studies have considered only lengths up to 0.64 m. The average relative uncertainty was determined to be ±5% with a maximum relative uncertainty of ±10% recorded at 0.2 m.

SIMULATION OF SENSOR RESPONSE

Using the linear sensor response function illustrated in *Fig. 2*, the question of sensor signal interpretation can now be addressed. The most important questions are:

(i) Can the sensor response distinguish between a defect-free mold filling and one with a manufacturing anomaly such as race tracking?
(ii) Can the sensor response identify what kind of defect is present?
(iii) Can an optimal sensor trajectory in a mold be identified that will provide the above information if only one sensor is used?

These questions were addressed by analyzing simulated sensor responses in a number of different simulated mold filling situations using the Liquid Injection Molding Simulation (LIMS) package developed at the University of Delaware (24). Times at which the flow front reached certain points lying along a predetermined sensor trajectory were noted. Using this information and the experimentally determined linear relation between the measured fluorescence intensity and length of sensor covered, the sensor response was obtained.

A flat, square mold of dimensions 1 m × 1 m × 0.01 m, with and without inserts, was used in all of the simulations. First, the mold filling of an isotropic preform was examined followed by the simulation of a mold filling with race tracking. Sensor trajectories considered are shown in *Fig. 3*. The injection gate is located at the center bottom edge and each mold filling simulation was performed under constant inlet pressure.

Simulations With No Inserts

Figure 4 illustrates the sensor response for the case of ideal filling with no inserts. Sensor 1 registers its first reading as soon as resin is injected because it intersects the source of the resin. There is a delay in the first response for Sensors 2 and 3 because it takes some time for the resin to reach them. In the initial stages of filling, the sensors are quickly covered which is indicated by the steep incline in the responses. As the flow front approaches the end of the mold, the rates at which the sensors are covered decrease and eventually coincide with the rate at which the mold is filled.

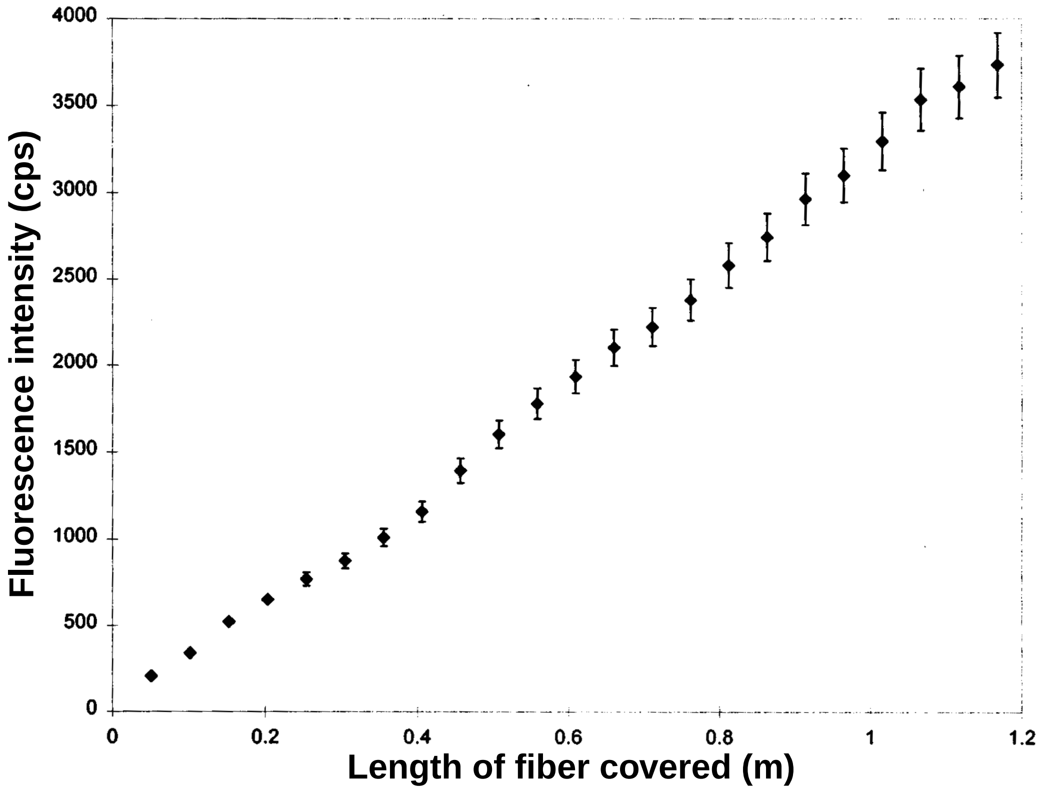

Fig. 2. Fluorescence intensity versus length of fiber covered for 10^{-5}mol/L aqueous Rhodamine; error bars indicate uncertainty in fluorescence intensity measurements.

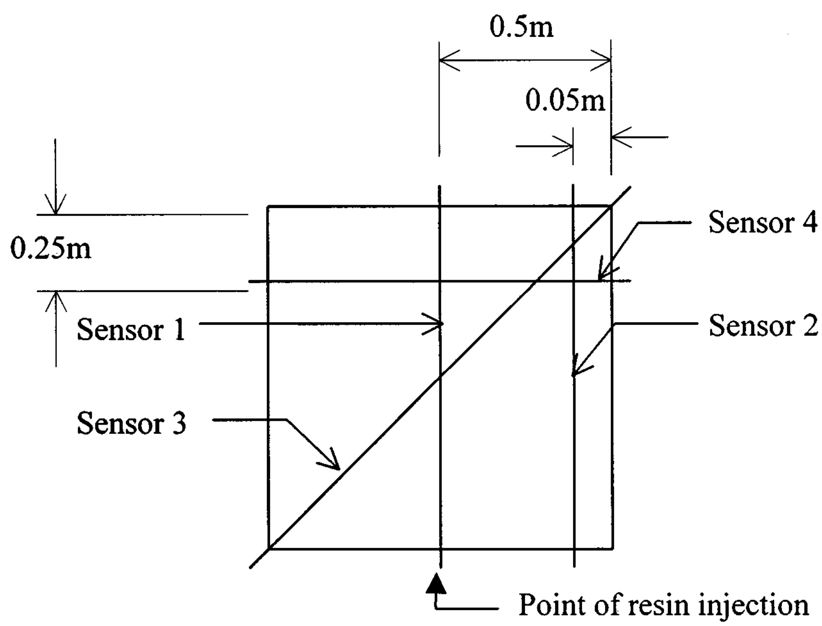

Fig. 3. Simulated sensor trajectories and resin injection points considered in the square mold.

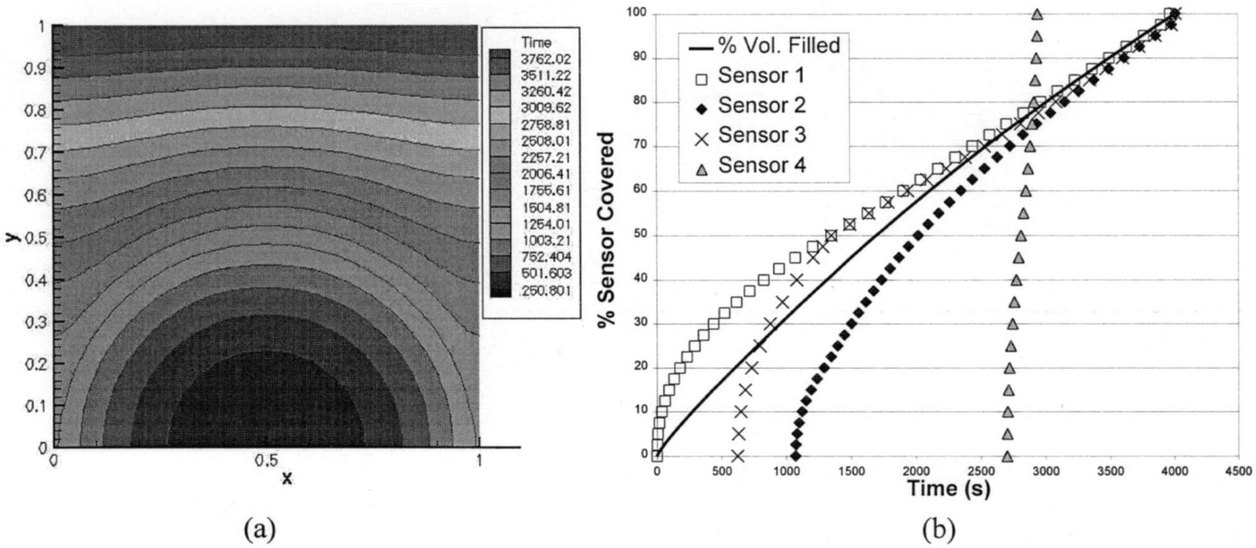

Fig. 4. (a) Simulated flow front progression for edge point injection in an isotropic mold, (b) Simulated sensor response, percentage fiber length covered versus time for constant inlet pressure.

In fact, all sensors, except for Sensor 4, which is oriented transverse to the direction of the advancing flow front, are completely covered at the same time as the mold is completely filled. Sensor 4 was almost instantaneously covered, suggesting an advancing flow front which is parallel to it. Both of these events indicate a flat flow front at the end of the mold, which is evident from *Fig. 4a.* If there are large differences in the times for Sensors 1, 2 and 3 for a given percent coverage, then the flow front is significantly curved in the y-direction as is the case in the first 1500 s of the filling process. Likewise, the smaller the differences, the flatter the flow front.

Data concerning the flow front progression in a normal mold filling will serve as the reference case for the results of the simulated responses for situations where there is race tracking in the mold. Race tracking usually occurs along the edges of the mold as a result of either an undersized or misaligned preform. Under these circumstances, there is a gap between the preform edge and the mold wall where resin moves more quickly compared to the resin speed within the preform.

In this study, the three race tracking cases shown in *Fig. 5* were considered. Note that race tracking can be beneficially used to fill a mold and is sometimes

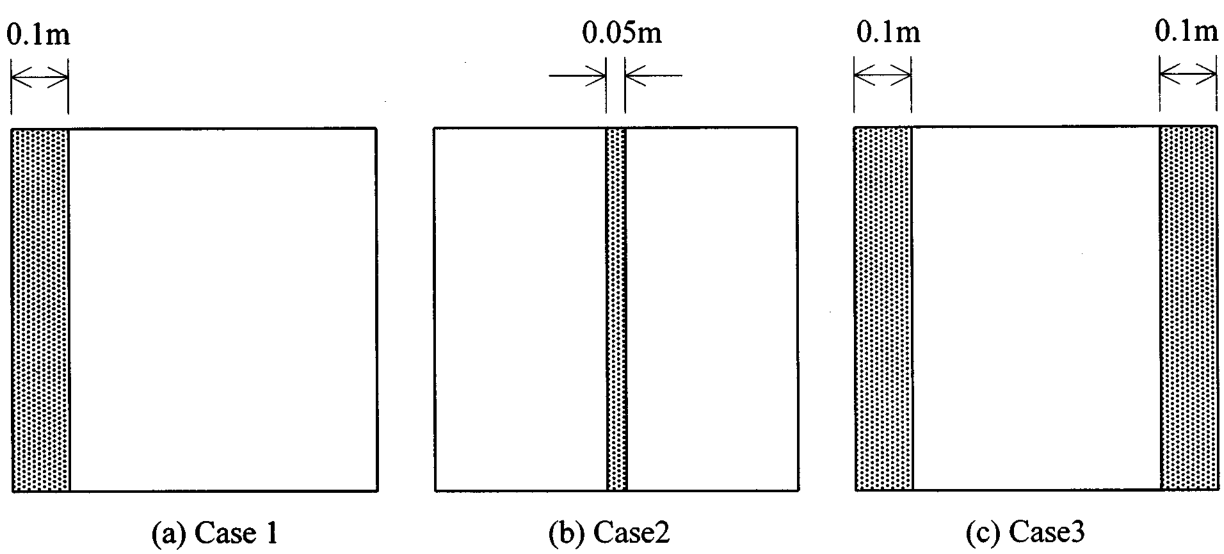

Fig. 5. Race tracking scenarios considered in this study (a) Case 1, race tracking along one edge, (b) Case 2, race tracking along the middle of the mold and (c) Case 3, race tracking along two opposite edges where shaded portions represent the race tracking elements in the mold.

deliberately introduced, especially in larger molds, to reduce the filling time and ensure that the more difficult places to reach are filled. Race tracking was simulated by setting the permeability in the race tracking areas to be 100 times that of the bulk permeability in the mold. In a study of the consequences of extreme edge effects, any gap exceeding a couple of millimeters would be sufficient to cause dramatic changes in the mold filling behavior. Hence, the widths of each race tracking region modeled, 0.1 m for both Cases 1 and 3, and only 0.05 m for Case 2, were selected based on numerical convenience.

As can be seen from *Fig. 6*, which contains the flow front progressions for each of the cases considered, the presence of race tracking can significantly alter the flow patterns from that of the idealized situation. Without venting the mold in the appropriate places, the probability of air entrapment would be high, for example, in the middle of the upper half of the mold for Case 3 where there is race tracking along the two opposite edges of the mold as shown in *Fig. 6d*. In *Fig. 7*, each graph shows the responses from one particular sensor trajectory in all of the mold filling cases examined here.

The first thing to note in *Figs. 7a–d* is, in general, all the sensors register their last readings at different times for each simulated case which indicates the flow front is no longer flat as in the defect-free case. Sensor Response 1 remains fairly unchanged from its normal response in Case 1 where resin race tracks along just one edge, but there are kinks in the response curve near the end of the mold filling in Case 3. For Case 2, race tracking along the middle of the mold, the sensor was covered in under 50 s as opposed to 4000 s under the idealized filling situation.

The time it takes for resin to cover Sensor 2 is reduced from 3200 s in the no race tracking case to 1200 s in Cases 1 and 3. In Case 2, the sensor is ac-

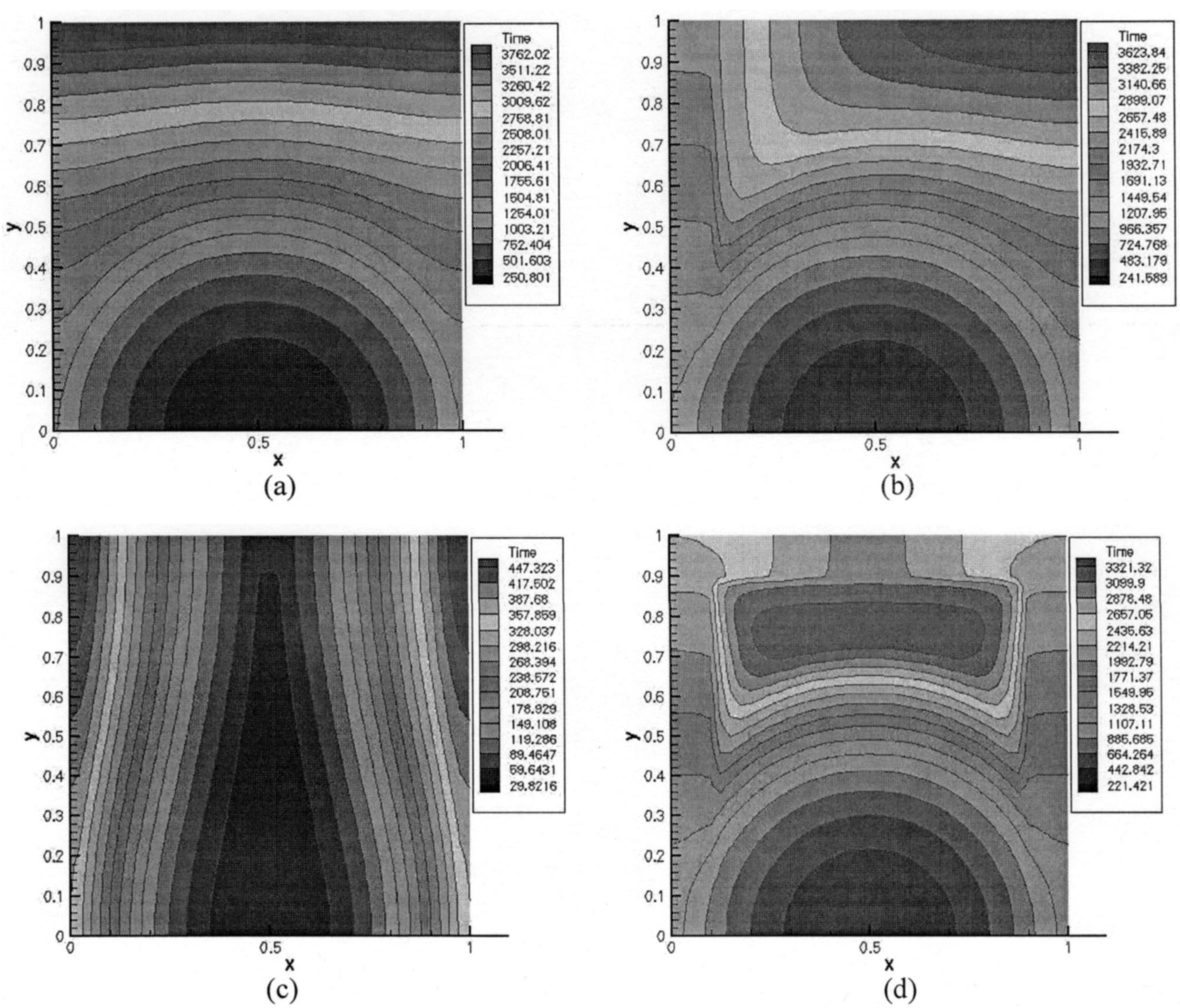

Fig. 6. Simulated flow front progression for edge point injection at constant inlet pressure with (a) no race tracking, (b) race tracking Case 1, on left edge (c) race tracking Case 2, in the middle; and (d) race tracking Case 3, on both left and right edges.

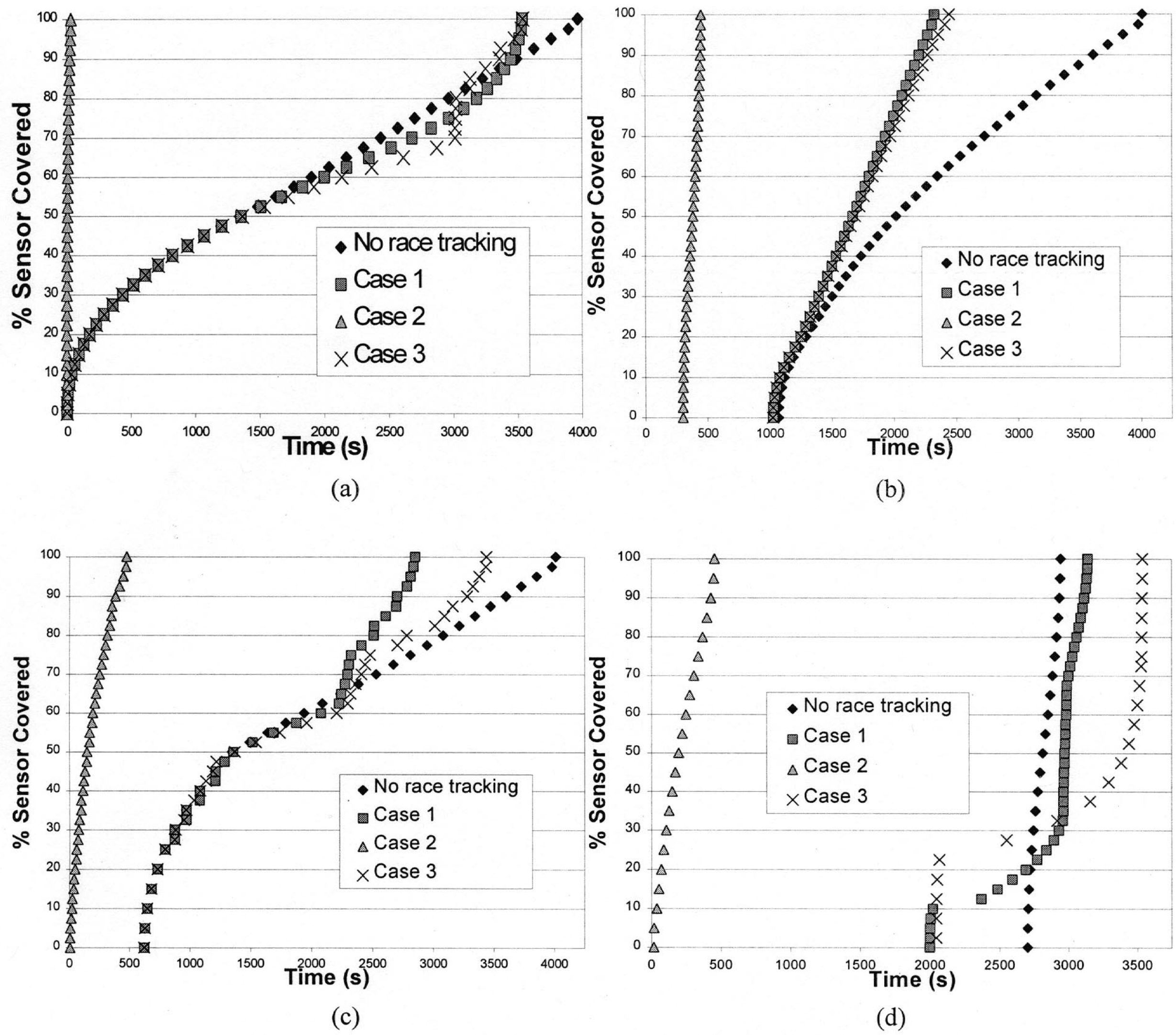

Fig. 7. Simulated sensor response for case with no race tracking and race tracking Case 1 (on left edge), Case 2 (in the middle) and Case 3 (on both left and right edges) for the flows illustrated in Figure 6; (a) the response from Sensor 1 in all four cases, (b) Sensor 2, (c) Sensor 3 and (d) Sensor 4.

tive for only 150 s, which means the flow front is nearly parallel to its trajectory. Although Sensors 1 and 2 are identically oriented within the mold, their responses are different from one another. For example, the starting times for each case are delayed because Sensor 2 is positioned further from the resin source. While Sensor Response 2 for Cases 1 and 3 are still similar to each other, they are now clearly distinguishable from the no race tracking case. This implies a sensor response is not only a function of its trajectory, but also its distance from the point of resin injection.

The first reading for Sensor 3 was registered about 600 s after resin was first injected into the mold for the defect-free situation and in Cases 1 and 3. For Case 2, the sensor came in contact with resin almost as soon as it was injected into the mold. Again, there are kinks in the responses towards the last stages of the mold filling for Cases 1 and 3, as was seen for Sensor 1 in Case 3.

The most interesting response is that of Sensor 4. In Case 1, the response is almost like a step function with two distinct vertical parts. The first, shorter vertical section corresponds to the race tracking part of the mold where the flow front is parallel to the alignment of Sensor 4. As resin slowly fills the rest of the mold, advancing ultimately to the top right corner, again the flow front gradually parallels the sensor's trajectory, producing the second vertical section of the response.

A similar result can be seen in Case 3 except that the height of the first vertical part is now twice that observed in Case 1. Moreover, in Case 3 there is a longer time lapse between the two vertical sections.

Consequently, the transition between the near horizontal step and the second vertical bit is more gradual. However, it should be pointed out that it is not possible just from looking at this sensor response alone to ascertain whether there is race tracking along both edges of the mold or just one really wide race tracking zone along one edge.

A sensor rating scheme was adhered to for the purpose of enabling the quantitative selection of the best sensor placement for detecting race tracking in this particular mold. The three criteria employed are as follows:

(i) How different are the race tracking sensor responses from the no race tracking case for each sensor trajectory?

(ii) How different are the responses from one another for each sensor trajectory?

(iii) How soon can these anomalies be identified?

From the experimental results, it was found there is on average a ±5% (maximum ±10%) uncertainty in the response from the EWF sensor. If these uncertainties are accounted for, the actual sensor responses lie within the uncertainty bands constructed about the simulated response as shown in *Fig. 8*, where the response of Sensor 3 is used for illustration. Here, the maximum uncertainty was used. Clearly, sensor uncertainty reduces the ability to differentiate one response from another.

Addressing the first criterion, the sensor response band from the no race tracking case is compared to the response bands from each of the three race tracking cases. For each comparison, the percentage of the sensor response over which the uncertainty bands do not overlap is determined. For instance, from *Fig. 8* it can be seen that 20% of the response for Case 1 does not overlap that of the no race tracking case. Responses from Case 2 and the no race tracking scenario do not overlap at all, even with uncertainty bands, so 100% of the sensor responses do not overlap. However, only 2% of the response for Case 3 does not overlap the no race tracking situation. Taking the average of these three values gives the score for the first criterion for Sensor 3 shown in *Table 1*. A higher score for this category indicates more distinct overall differences between the race tracking responses and the defect-free one.

Not only do the responses need to be different from the no race tracking response, they also have to be sufficiently different from one another so that it is possible to distinguish the response for one race tracking scenario from another. The score for the second criterion reflects how well a sensor distinguishes the various race tracking cases. Now, the degree to which the uncertainty bands overlap in the remaining three possible combinations of unique pairs must be considered as well.

Again for Sensor 3, the response for Case 2 does not overlap that for Case 1, nor does it overlap with the response for Case 3, so the difference is 100% for both of those comparisons. In contrast, only 12% of the response from Case 1 and Case 3 do not overlap. The score shown for Sensor 3 under the second criterion is the average of all of the above six values since the three race tracking cases and no race tracking case are under consideration here. Again, a high score is more desirable because it means that the responses

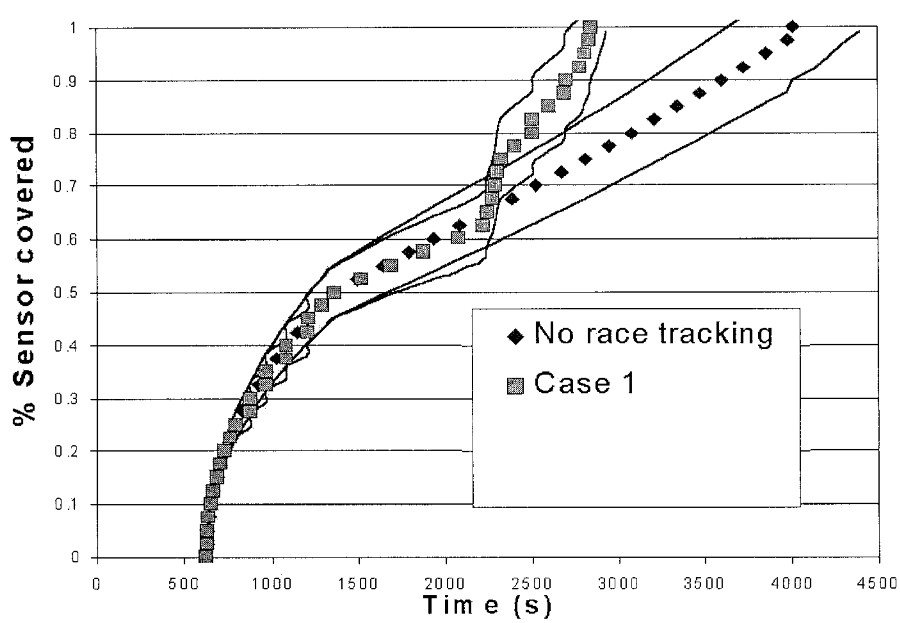

Fig. 8. Simulated sensor response for case with no race tracking and Case 1 (race tracking on left edge) for Sensor 3 with ±10 % uncertainty bands constructed about the simulated responses.

Table 1. Sensor Ratings Summary for Race Tracking Simulations.

Sensor	Uncertainty Level	Criteria (i)	Criteria (ii)	Criteria (iii)	Total
1	±10%	0.325	0.488	0.309	0.374
1	±5%	0.382	0.520	0.318	0.407
1	0%	0.699	0.776	0.590	0.689
2	±10%	0.894	0.780	1.000	0.892
2	±5%	0.984	0.825	1.000	0.936
2	0%	1.000	0.971	1.000	0.991
3	±10%	0.407	0.557	0.335	0.433
3	±5%	0.488	0.622	0.562	0.557
3	0%	0.715	0.776	0.575	0.689
4	±10%	0.959	0.963	1.000	0.974
4	±5%	0.984	0.984	1.000	0.989
4	0%	1.000	1.000	1.000	1.000

for the different race tracking scenarios are clearly discernible from each other. Hence, it will be possible to identify where race tracking is occurring within the mold.

The sooner an anomaly is detected in the mold, the more time there is available for the operator to take necessary corrective measures and possibly prevent the part from being rejected. Hence, early identification of an anomalous situation is far more valuable than an indication towards the end of the filling process. To obtain a measure of how well the sensor performed under the third criterion, the lowest percent sensor covered at which the response bands of the race tracking and defect-free situations do not overlap is noted. This value was then subtracted from unity and cubed to yield a score for that particular comparison. Subtraction from unity makes a higher score better for Criterion 3, which is consistent with the scoring for Criteria 1 and 2. Cubing that result reflects the importance of early detection, but the cubic power is arbitrary.

For example, in *Fig. 8*, the Sensor Response 3 for Case 1 overlaps that of the no race tracking case up till 82.5% coverage, which would give a score of 0.005. From *Fig. 7c*, Case 2 never overlaps with the defect-free situation and so it gets a score of unity. On the other hand, the uncertainty bands for Case 3 and the normal response separate only at the very last point and, hence, it gets a zero. The average of these three values yields the final score for the third criterion as presented in *Table 1*.

Finally, an overall rating of the sensor's performance is obtained by averaging the scores for the three criteria. The responses from the other sensors are rated in the same way to yield the values presented in *Table 1*. According to this rating scheme, Sensor 1 did rather poorly, largely due to its responses in Cases 1 and 3 being so similar to that of the no race tracking scenario. Sensor 4 is the best trajectory to use in detecting these three specific race tracking situations as it has the highest score in all four categories.

Sensor scores for the situation where there is no uncertainty in the sensor output measurement are also presented in *Table 1*. As expected, the sensors scored higher in the 0% uncertainty case than in the ±10% uncertainty case but the ranking of sensor performance remains unchanged, that is, Sensor 4 still has the highest score followed by Sensor 2 and then Sensors 1 and 3. Ratings for a ±5% uncertainty are also included as an intermediate case between the two extremes. The values for this case lie in between the corresponding values of the other two situations.

Mold with Double Inserts

This study was extended to a more complicated mold geometry to determine if a single line sensor could still provide useful information under more realistic manufacturing conditions. To this end, a square mold with two inserts was used, as shown in *Fig. 9*, and the race tracking cases indicated in *Fig. 10* were studied. Here, the widths of the edge effects are 0.04 m in all of the cases considered. Again, this value was picked based on numerical convenience.

Only the sensor positions indicated by solid lines depicted in *Fig. 9b* were considered in the filling simulations of this particular mold geometry. Sensors 1 and 3 shown in the dashed lines were not considered because the mold inserts intersected parts of those sensor trajectories and, hence, it would not be physically feasible to place a sensor in those locations without bending it. Again the responses from the sensors in various race tracking scenarios will be compared to their response in the idealized mold filling case. *Figures 11* and *12* illustrate the flow patterns and sensor responses from simulations using this mold geometry.

In race tracking Case 5 where there is race tracking only along the insert edges, Sensor 5 first came in contact with the resin 750 s after the commencement of resin injection in the mold, instead of 600 s as in the no race tracking case. However, the response is similar to the defect-free case except for the two step-like parts in the race tracking curve. The entire length of Sensor 5 was covered in less than 120 s after resin was injected into the mold in both race tracking Case 4, where there was race tracking along only the outer edges, and Case 6, which has race tracking along all mold edges. The responses in both of these cases are also very similar to one another.

Resin first reaches Sensor 7 at an earlier time in all three cases as compared to the defect-free scenario as

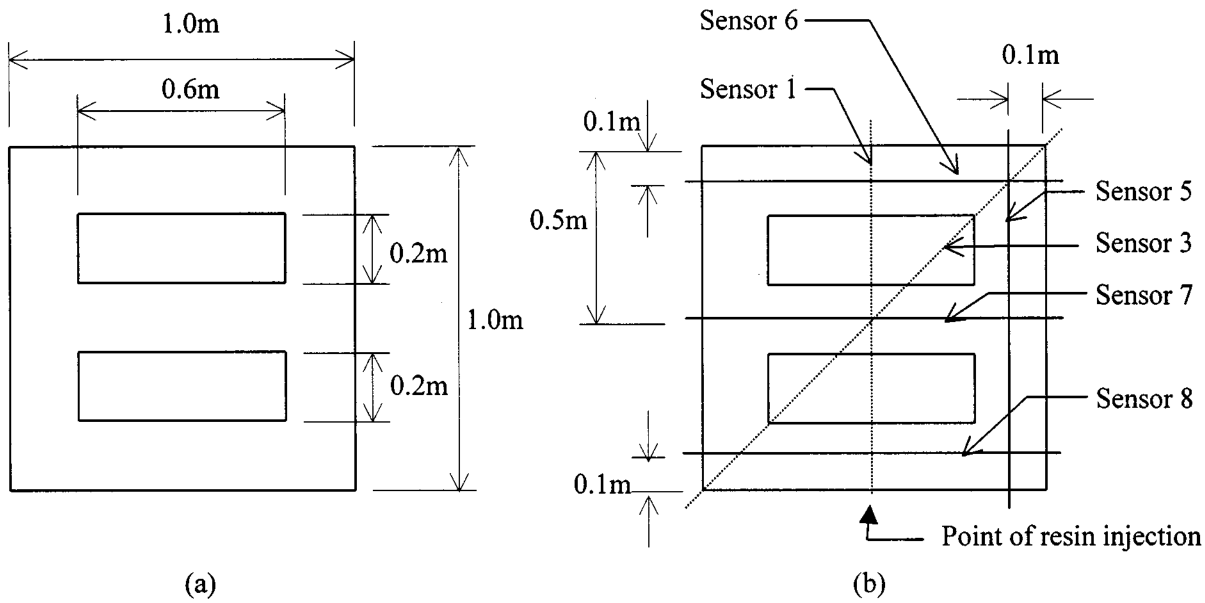

Fig. 9. Square mold with double inserts and sensor trajectories considered.

depicted in *Fig. 11a*. In Case 5, the flow front arrives parallel to 70% of the sensor, and, hence, the first 70% of it was covered in 10 s as compared to 750 s in the normal filling situation. For Case 4, only the first 10% of the sensor is covered instantaneously. A combination of both effects from Cases 4 and 5 can be observed in Case 6 where race tracking occurs at all mold edges. In Case 6, the initial 10% of the sensor is covered at once due to race tracking along the mold edges while resin covers the last 70% within 10 s as a result of the race tracking along the insert edges.

The response from Sensor 6 is similar to that of Sensor 7 but it takes place at a delayed time since it is positioned further from the resin injection source. While it may appear in *Fig. 12b* that the sensor responses for Cases 4 and 6 overlap substantially, and hence, the scores for Criterion 2 should not be so high, looking at the two responses on an expanded time scale in *Fig. 13* shows that not to be the case. Sensor 8 is covered in less than 15 s in Cases 4 and 6, while in Case 5, the sensor is active for 1200 s. It normally takes 750 s to completely cover the sensor. Sensor responses for Cases 4 and 6 were identical.

The same rating scheme described in the previous section was applied to the sensor trajectories considered above and the results are summarized in *Table 2*.

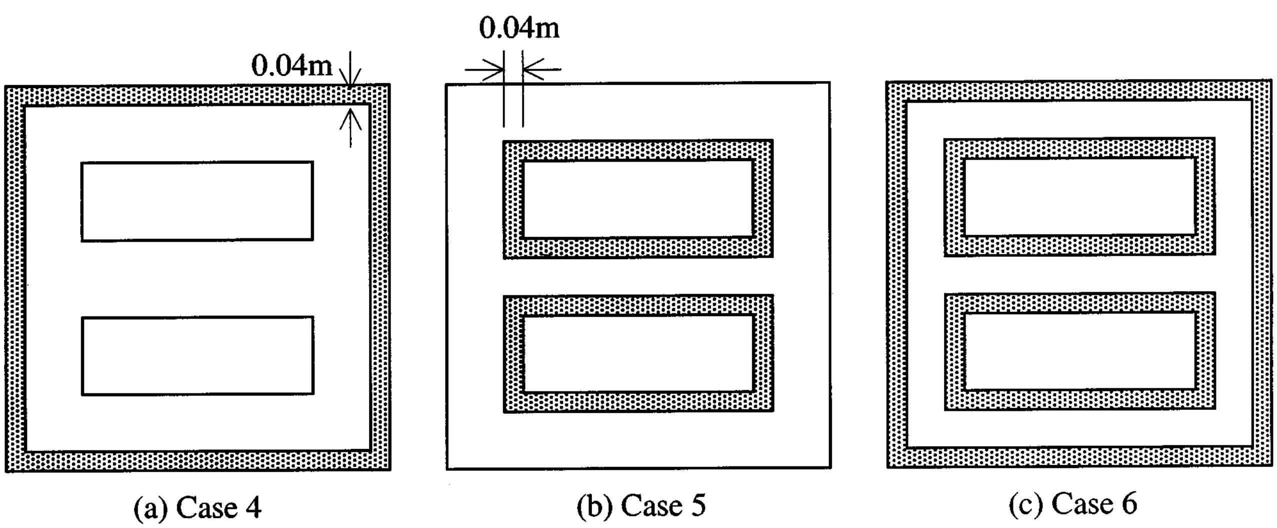

Fig. 10. Race tracking cases considered for mold with double inserts; (a) Case 4, race tracking along outer edges; (b) Case 5, race tracking along insert edges and (c) Case 6, race tracking along all edges where shaded portions represent the race tracking elements in the mold.

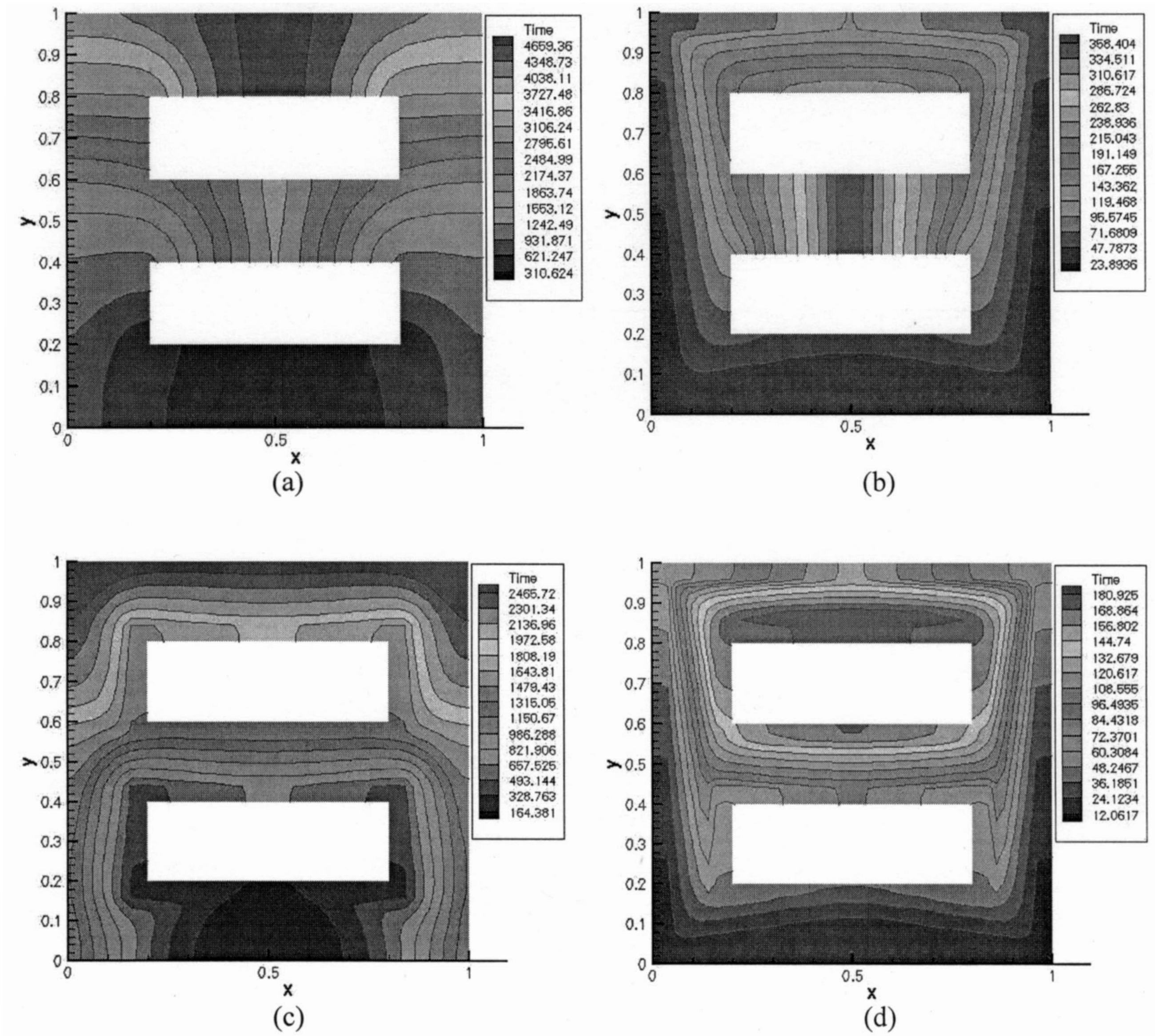

Fig. 11. Simulated flow front progression for edge point injection at constant inlet pressure with (a) no race tracking, (b) race tracking on outer edges, Case 4; (c) race tracking along the insert edges, Case 5 and (d) race tracking on all edges, Case 6.

From this *Table*, Sensor 7 performed only marginally better than Sensor 6 for detecting race tracking in the mold with double inserts, so either one of these may be selected as the best sensor for this purpose. However, in general, there was no disparity in the performances of these four sensor trajectories as was seen in the sensor trajectories considered for the simple square mold. They all did well in fulfilling the three criteria.

CONCLUDING REMARKS

The EWF intensity was experimentally determined to be linearly proportional to the length of sensor covered for fiber lengths up to 1.17 m. This relation was incorporated into the simulation work to help select the optimal placement of the sensor in the mold.

From the above discussion, it is clear that resin flow front progression within a mold can be deduced from a combination of sensor responses from several different locations. However, it is possible to detect race tracking within a mold and to some extent also identify where it takes place with only a single sensor.

A sensor ratings scheme such as the one proposed in this study serves as a useful tool in the selection of the best sensor trajectory that would convey the most timely information concerning the mold filling. This rating scheme has also been successfully applied to the mold with double inserts filling simulations. Nonetheless, it is acknowledged that only a very limited number of possible race tracking scenarios and sensor placements have been explored in this paper and the choices identified here may not be the optimum.

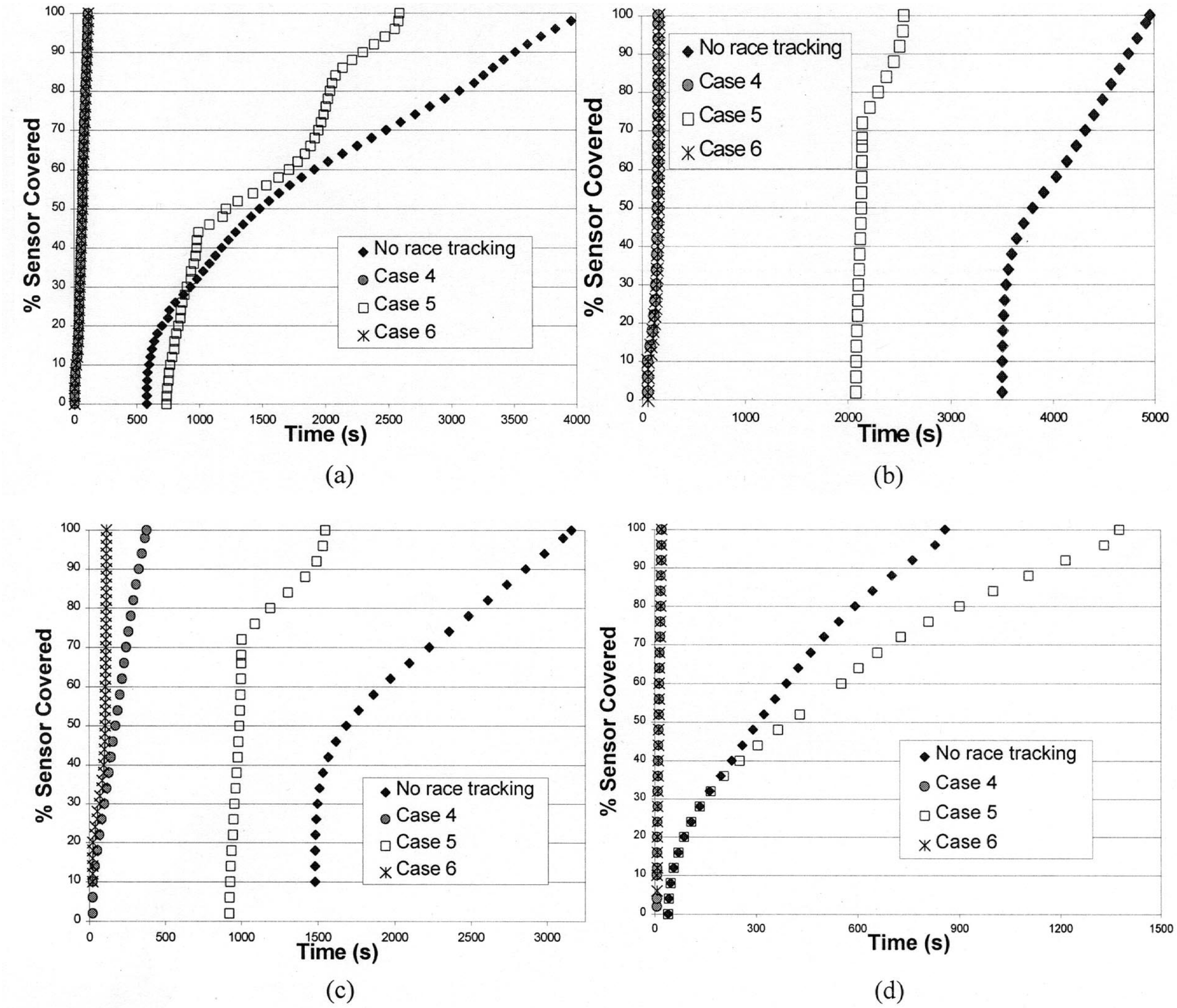

Fig. 12. Simulated sensor response for normal case with no race tracking in mold with double inserts and Case 4 (on outer edges), Case 5 (on insert edges) and Case 6 (on all mold edges) with edge point injection at constant inlet pressure) for the flows illustrated in Figure 10; (a) the response from Sensor 5 in all four cases, (b) Sensor 6, (c) Sensor 7 and (d) Sensor 8.

Fig. 13. Simulated sensor response for Sensor 6, refer to Figure 12b, on an expanded timescale for Case 4 (on outer edges) and Case 6 (on all mold edges) with edge point injection at constant inlet pressure.

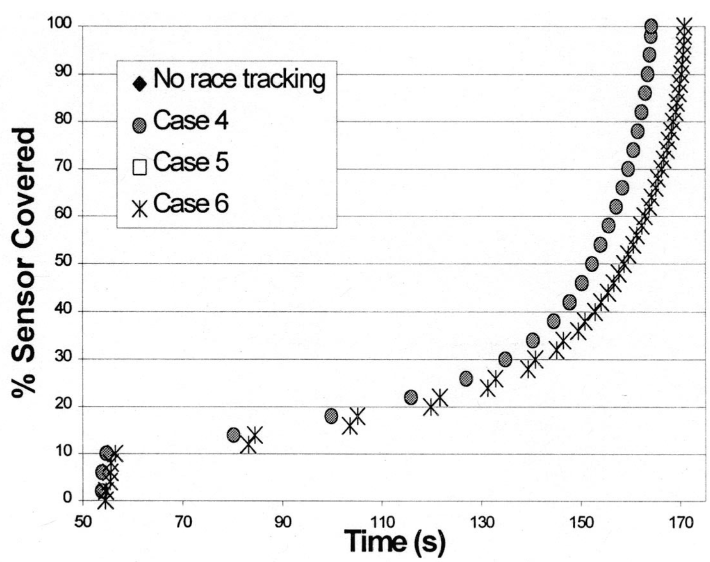

Table 2. Sensor Ratings for Sensor Trajectories Considered in Double Insert Mold.

Sensor	Uncertainty Level	Criteria (i)	Criteria (ii)	Criteria (iii)	Total
5	±10%	0.889	0.778	1.000	0.889
5	±5%	0.935	0.804	1.000	0.913
5	0%	0.993	0.931	1.000	0.975
6	±10%	1.000	0.928	1.000	0.976
6	±5%	1.000	0.967	1.000	0.989
6	0%	1.000	0.977	1.000	0.992
7	±10%	1.000	0.941	1.000	0.980
7	±5%	1.000	0.954	1.000	0.985
7	0%	1.000	0.974	1.000	0.991
8	±10%	0.824	0.745	0.695	0.755
8	±5%	0.850	0.758	0.714	0.774
8	0%	0.902	0.830	0.791	0.841

Curved sensor trajectories that trace two or more mold edges would certainly yield significantly more information on the flow pattern than any of the sensor placements investigated in this paper. Furthermore, the three criteria listed may not form the complete set of criteria for this selection process and there may exist others which have not yet been recognized. Depending on how the information from a study like this one is to be used, each criterion could also be assigned a weighting factor based upon the degree of importance of that particular criterion in the selection process.

Although we are able to differentiate between a defect-free mold filling and one with race tracking, the responses do not always indicate the exact location of the problem in the mold. For example, Sensor Response 1 for race tracking along the edge of a square mold may show us there is race tracking but it does not tell us whether it is occurring along the upper or lower edge of the mold or both.

In conclusion, choosing the best sensor trajectory still requires knowledge of the flow pattern and sensor response expected in a defect-free filling and that of the anticipated defective filling.

REFERENCES

1. S. G. Advani, M. V. Bruschke. and R. S. Parnas, in *Flow and Rheology in Polymer Composites Manufacturing*; S. G. Advani, ed., Elsevier Applied Science Publishers, New York (1994).
2. C. Binetruy, B. Hilaire, and J. Pabiot, *Automated Compos.*, Sept. (1995).
3. Y.-T. Chen, H. T. Davis, and C. W. Macosko, *AIChE J.*, **41**, 2261 (1995).
4. A. Kikuchi, E. Higuerey, and J. Coulter, *Trans. ASME J. Eng. Mater. Technol.*, **117**, 89 (1995).
5. S. M. Milkovich, *State-of-the-Art Review on the Use of Sensors and Controls as it Relates to Resin Transfer Molding (RTM) of Composite Materials*, MTIAC SOAR-98-01 (1998).
6. N. Patel, V. Rohatgi, and L. J. Lee, *Polym. Compos.*, **14**, 161 (1993).
7. S. H. Ahn, W. I. Lee, and G. S. Springer, *J. of Compos. Mater.*, **29**, 714 (1995).
8. S. Bickerton, H. Stadfeld, K. V. Steiner, and S. G. Advani, *Proc. 13th ASC Techn. Conf. Compos. Mater.*, 232 (1998).
9. M. V. Bruschke and S. G. Advani, *Polym. Compos.*, **11**, 398 (1990).
10. B. K. Fink, S. M. Walsh, D. C. DeSchepper, J. W. Gillespie Jr., R. L. McCullough, R. C. Don, and B. J. Waibel, *Proc. 1995 ASME MD Inter. Mechanical Eng. Congress and Exposition*, **69**, 999 (1995).
11. D. A. Klosterman and T. E. Saliba, *38th Inter. SAMPE Symp.*, **38**, 1322 (1993).
12. D. E. Kranbuehl, P. Kingsley, S. Hart, G. Hasko, B. Dexter, and A. C. Loos, *Polym. Compos.*, **15**, 299 (1994).
13. R. E. Lyon, K. E. Chike, and S. M. Angel, *J. Appl. Polym. Sci.*, **53**, 1805 (1994).
14. N. Patel, V. Rohatgi, and L. J. Lee, *Polym. Compos.*, **14**, 161 (1993).
15. R. S. Parnas and F. R. Phelan, Jr., *36th Inter. SAMPE Symp.*, 506 (1991).
16. F. R. Phelan, Jr., *Proc. 7th ASC Techn. Conf.*, 90 (1992).
17. T. Sadiq, R. Parnas, and S. G. Advani, *24th Inter. SAMPE Techn. Conf.*, **24**, T660 (1992).
18. A. D. Schwab, R. L. Levy, and G. G. Glover, *Polym. Compos.*, **17**, 312 (1996).
19. D. L. Woerdeman, K. M. Flynn, J. P. Dunkers, and R. S. Parnas, *J. Reinforced Plast. Compos.*, **15**, 922 (1996).
20. R. J. Young, *J. Microscopy*, **185**, 199 (1997).
21. A. A. Skordos, P. I. Karkanas, and I. K. Partridge, *Novel Dielectric Sensor Setup for Flow and Cure Monitoring in Resin Transfer Molding*, Proceedings of the 12th International Conference on Composite Materials (1999).
22. Z. Cai and D. J. Lawrie, *24th Inter. SAMPE Techn. Conf.*, T675 (1992).
23. Y. M. Ismail and G. S. Springer, *J. Compos. Mater.*, **31**, 954 (1997).
24. P. Simacek, E. M. Sozer, and S. G. Advani, *User Manual for Drape 1.1 and LIMS 4.0*; CCM Report 98–101.
25. F. Trochu, R. Gauvin, D. M. Gao, and J. Boudreault, *J. Reinforced Plast. Compos.*, **13**, 262 (1994).
26. C.-J. Wu and L.-W. Huorng, *Polym. Eng. Sci.*, **35**, 1272 (1995).
27. J. R. Bernstein and J. W. Wagner, Rev. Scientific Instrumentation, **68**, 2156 (1997).
28. J. P. Dunkers, K. M. Flynn, and M. T. Huang, *Proc. SPE ANTEC '97*, 2451 (1997).
29. Y. M. Liu, C. Ganesh, J. P. H. Steele, and J. E. Jones, *J. Compos. Mater.*, **3**, 87 (1997).
30. R. A. Neff, D. L. Woerdeman, and R. S. Parnas, *Polym. Compos.*, **18**, 518 (1997).
31. F. W. Wang and B. M. Fanconi, *In-situ Characterization of the Interface of Glass Reinforced Composites*, U.S. Army Research Office (1987).
32. D. L. Woerdeman and R. S. Parnas, *Plast. Eng.*, October 1995, p. 25.
33. D. L. Woerdeman and R. S. Parnas, *Proc. SPE ANTEC '95*; **II**, 2805 (1995).

34. D. L. Woerdeman, J. L. Spoerre, K. M. Flynn, and R. S. Parnas, *Polym. Compos.*, **18**, 133 (1997).
35. D. L. Woerdeman, K. M. Flynn, and R. S. Parnas, *Automated Composites*, Sept. (1995).
36. D. L. Woerdeman, *Characterization of the Liquid Molding Process of Composite Manufacturing, PhD. Thesis*, John Hopkins University (1996).
37. G. G. Guilbalt, *Practical Fluorescence: Theory, Methods and Techniques*, 2nd Edition, Marcel Dekker Inc., New York (1990).
38. N. J. Harrick, *Internal Reflection Spectroscopy*, Harrick Scientific Corporation, New York (1987).
39. J. Hecht, *Understanding Fiber Optics*, Second Edition; Sams Publishing (1993).
40. D. A. Krohn, *Fiber Optic Sensors: Fundamentals and Application, 2nd Edition*, Instrument Society of America, Research Triangle Park, NC (1992).
41. J. R. Lakowicz, Z. Gryczynski, and I. Gryczynski, *Photochemistry and Photobiology*, **64**, 5635 (1995).
42. D. Marcuse, *The Bell System Technical Journal*, **55**, 1463 (1976).
43. A. Messica, A. Greenstein, and A. Katzir, *Appl. Optics*, **35**, 2274 (1996).
44. O. S. Wolfbeis, *Fiber Optic Chemical Sensors and Biosensor, Vol. 1*; CRC Press Inc., Boca Raton, FL (1991).
45. C. Egami, K. Takeda, M. Isai, and M. Ogita, *Optics Communications*, **122**, 122 (1996).
46. V. Ruddy, B. D. MacCraith, and J. A. Murphy, *J. Appl. Phys.*, **67**, 376 (1996).
47. J. D. Andrade, R. A. van Wagenen, D. E. Gregonis, K. Newby, and J. N. Lin, IEEE Trans. Electron Devices, **ED–132**, 1175 (1985).
48. E. F. Carome, G. A. Coghlan, C. N. Sukenik, and J. E. Zull, *Sensors and Actuators, B*, **13–14**, 732 (1993).